1-1-2006

The Effect of Residual Stress on the Fatigue Crack Growth Behavior of Al-Si-Mg Cast Alloys - Mechanisms and Corrective Mathematical Models

Diana A. Lados
Worcester Polytechnic Institute, lados@wpi.edu

Diran Apelian
Worcester Polytechnic Institute, dapelian@wpi.edu

The Effect of Residual Stress on the Fatigue Crack Growth Behavior of Al-Si-Mg Cast Alloys—Mechanisms and Corrective Mathematical Models

DIANA A. LADOS and DIRAN APELIAN

The fatigue crack growth (FCG) behavior of various types of alloys is significantly affected by the presence of residual stress induced by manufacturing and post-manufacturing processes. There is a qualitative understanding of the effects of residual stress on fatigue behavior, but the effects are not comprehensively quantified or accounted for. The difficulty in quantifying these effects is largely due to the complexity of residual-stress measurements (especially considering that parts produced in similar conditions can have different residual-stress levels) and the lack of mathematical models able to convert experimental data with residual stress into residual-stress-free data. This article provides experimental, testing, and mathematical techniques to account for residual-stress effects on crack growth rate data, together with two methods for eliminating residual stresses in crack growth test specimens. Fracture-mechanics concepts are used to calculate, in simple and convenient ways, stress-intensity factors caused by residual stresses. The method is advantageous, considering that stress-intensity factors are determined before the actual test is conducted. Further on, residual-stress-intensity factors are used to predict the residual-stress distribution in compact tension (CT) specimens prior to testing. Five cast Al-Si-Mg alloys with three Si levels (in unmodified (UM) as well as Sr-modified (M) conditions) were analyzed both with and without residual stress. Fatigue cracks are grown under both constant stress ratio, $R = 0.1$, and constant maximum stress-intensity factor, K_{max} = const., conditions. The mechanisms involved in crack growth through residual-stress fields are presented.

I. INTRODUCTION AND BACKGROUND

RESIDUAL stresses are self-equilibrating internal or locked-in stresses remaining in a material that is free of applied (external) forces, external constraints, and temperature gradients.[1,2] In most cases, residual stresses are an undesired result of processing, and they persist in the material unless eliminated through stress-relieving techniques. Residual stresses are commonly found in weldments, complex forged and extruded parts, and castings, especially when the cast parts have been heat treated. In some cases, compressive residual stresses are purposely introduced near the surface (*e.g.*, shot peening), to improve fatigue life. The major difference between these cases consists in the type of residual stress (compressive, which retards fatigue crack growth, or tensile, which accelerates fatigue crack growth) and the knowledge of the residual-stress level. When residual stress is a random effect of various processing conditions, the residual-stress level is difficult to predict; on the other hand, when residual stress is purposely introduced, it is known and quantified. In general, residual stresses may develop in the material as a response to plastic-deformation processes such as machining, grinding, and forming; a phase transformation that is induced upon cooling, in which parent and product phases have different densities or crystal structures; or the nonuniform cooling of a piece that was fabricated or processed at elevated temperatures. The most common severe residual macrostresses, however, are introduced by nonuniform cooling. Residual stresses are found in all alloy systems: aluminum alloys, superalloys, titanium alloys, steels, *etc*.

Knowledge of the residual-stress level in the component is very important, particularly when techniques to account for it are developed. There are several methods (nondestructive, partly destructive, and destructive) used to measure initial residual-stress fields in materials. All stress measurements are based on the evaluation of the actual strain or changes in the strain, and they can be either qualitative or quantitative. The most commonly used stress-measuring techniques have been reviewed,[3,4,5] and they are listed here to emphasize their diversity: photo-stress coatings, ultrasonic (acoustics), electromagnetic (including Barkhausen noise analysis), photoelasticity, X-ray diffraction, neutron diffraction, hole drilling, positron annihilation, nuclear hyperfine (including Mossbauer), spectroscopy, chemical etching, sectioning strain-gaged samples, and indentation and microhardness mapping. The technique of X-ray diffraction is recognized to be the only truly nondestructive technique that is reliable. However, its severe limitations are that it can be applied nondestructively only on the surface, and it is a long and expensive procedure. The difficulties and limitations associated with all these techniques reduce the ability to accurately measure residual stresses.

Despite these difficulties, determining the presence, magnitude, and distribution of residual stresses is vital for the correct interpretation of FCG experimental data and, implicitly, for real service-life predictions. It has been known for a long time that residual stress has a strong impact on FCG behavior, *da/dN vs* ΔK.[6–17] Even if residual stresses affect only mean stresses or stress ratios, they do significantly influence crack initiation, propagation, and closure.[14,17–22] The approach most frequently used to account for the effect of residual stress on crack growth superposes the stress-intensity factors from

DIANA A. LADOS, Research Scientist, and DIRAN APELIAN, Professor, are with the Metal Processing Institute, Worcester Polytechnic Institute, Worcester, MA 01609. Contact e-mail: lados@wpi.edu

Manuscript submitted February 21, 2005.

the initial residual stress and the applied loads, *i.e.*, $K_{eff} = K_{res} + K_{app}$;[6,9,10,14,15,17] however, at minimum load, when cracks are only partially opened, the superposition model can become invalid due to nonlinear contact of the mating faces. Corrective methods for residual-stress compensation based on linear elastic fracture mechanics concepts are most desirable, so that existing *da/dN*-ΔK data with residual stress may be directly adjusted and further utilized for residual-stress-free applications. As a result, residual-stress-intensity factors, K_{res}, are of prime interest because they can be used directly in FCG and fracture relationships. Residual-stress-intensity factors, K_{res}, have been calculated for several crack types and crack face stress distributions mostly using weight function models (WFM),[6,9,10,14,15,17] a method that requires prior knowledge of the residual-stress profile.

More recently, a simple and promising technique was developed based on successive extensions of the compact tension (CT) specimen notch, while the changes in strain on the back face of the specimen are captured. This fracture-mechanics-based technique evolved from previous work,[23] and developed into the cut-compliance method[24] successfully applied in other studies.[25] This new technique provides residual-stress-intensity factors directly from the measured strains, without first solving for the residual stresses. Subsequently, residual-stress profiles can be back-calculated, using weight functions. The major assumption here is that residual stresses do not change or redistribute with the crack growth. Depending on the crack closure mechanisms (residual stress, roughness, plasticity, and oxides), this assumption can potentially overestimate the effect of residual stresses on fatigue crack growth. However, even if changes in the magnitude and redistribution of residual stresses can theoretically occur during crack growth, residual-stress-induced closure and roughness-induced closure interact in a complex, nonlinear fashion at low stress ratios. This interaction may, in fact, overcome the magnitude change and residual-stress redistribution.

This study addresses residual stresses resulting from quenching during the heat treatment (T61) of Al-Si-Mg alloys. Three different ways of deriving residual-stress-free data from FCG experiments are presented. First, the behaviors of CT specimens with high residual stress (HRS) and low residual stress (LRS) are analyzed, and residual-stress-free fatigue crack growth thresholds are determined from experimental data with different degrees of residual stress. Second, two methods to mathematically compensate for the presence of residual stress are developed. Third, two methods to produce residual-stress-free samples are introduced, and the corrective methods are verified. Finally, a method to predict residual-stress distribution without physical measurements, simply by using K_{res} data and weight functions, is addressed using numerical integration.

II. EXPERIMENTAL PROCEDURE

A. *Alloys, Casting Procedure, and Heat-Treating Conditions*

Cast Al-Si-0.45 pct Mg specimens, with Si in both unmodified (UM) and Sr-modified (M) conditions were tested. The levels of Si used in this work are 1, 7, and 13 pct. The grain size of all alloys was kept constant (~280 μm) by appropriate additions of an Al-5 pct Ti-1 pct B master alloy, and Sr-modification was done using an Al-10 pct Sr master alloy. High-purity alloys were used so that all the other elements were kept at very low levels, <0.002 pct; the Fe concentration was <0.02 pct. Secondary dendrite arm spacing (SDAS) was controlled for all alloys in the range 20 to 30 μm. For the fatigue growth studies, CT specimens were prepared using a specifically designed sand mold containing central top and bottom gray cast iron chills, to insure the desired SDAS throughout the region of interest. The original castings used to prepare the CT samples had the following dimensions: 112 × 112 × 20.5 mm (4.4 × 4.4 × 0.8 in.).

Most commercial aluminum alloys reach a desired level of strength through heat treatment, one of the most significant sources of residual stress. A solution-treatment stage is followed by a quenching procedure from a solution-treatment temperature of around 538 °C. The residual-stress level introduced in the samples when room-temperature (RT) water quench is used is very high. The explanation for this phenomenon is that during quenching, the surfaces of the samples cool faster than their interiors, and temperature gradients are created, which causes different regions of the sample to contract at different rates. During the latter stages of cooling, these gradients disappear, but their presence sets up an uneven distribution of residual stresses. These residual stresses are compressive on the surface of the sample and tensile in the center. After quenching, the tensile and compressive stresses present in the sample are balanced, and the total net stress equals zero for the whole sample. The aging treatment applied after quenching enhances the strength of the part, through the development of strengthening precipitates, but it has no significant effect on residual stresses.

Two T61 heat-treating procedures were used and these are described subsequently. Both treatments resulted in distinctly different Si morphologies between the UM and Sr-M alloys, and produced a consistent matrix microhardness in all the alloys. However, the level of residual stress induced in the samples during the two heat treatments was significantly different.

The first heat-treatment procedure (RT water quench) consisted of the following steps:

(a) solution treatment for 1.5 hours at 538 °C (1000 °F),
(b) water quenching in agitated water at RT,
(c) natural aging for 12 hours, and
(d) artificial aging for 12 hours at 155 °C (311 °F).

The residual-stress level introduced in the samples by the RT water quench was found to be very high. Therefore, an alternative heat treatment was designed to alleviate the residual-stress contribution and to provide residual-stress-free CT specimens.

The second heat-treatment procedure (uphill quench) consisted of the following steps (details about the procedure and the operating mechanisms are presented elsewhere):[26]

(a) solution treatment for 1.5 hours at 538 °C (1000 °F),
(b) boiling-water quenching for 15 minutes,
(c) liquid N_2 immersion for 30 minutes,
(d) boiling-water reverse quenching for 15 minutes,
(e) natural aging for 12 hours, and
(f) artificial aging for 12 hours at 155 °C (311 °F).

Samples were vertically introduced into the quenching media and the sample transfer time from one medium to another was less than 2 seconds.

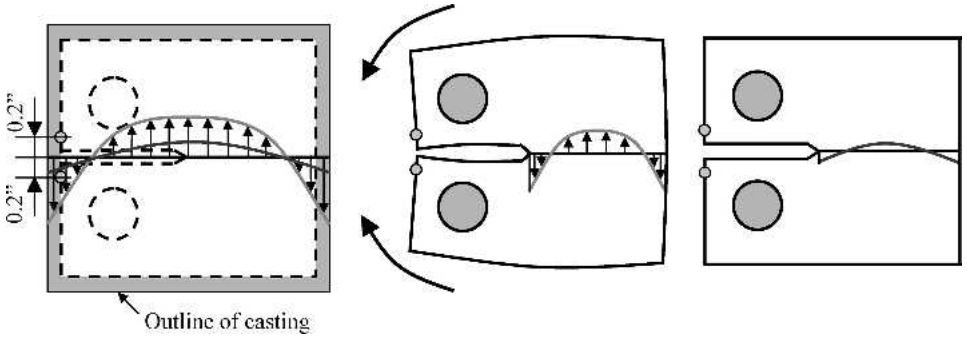

Fig. 1—(*a*) Scribed samples with HRS and LRS after machining and before notching, (*b*) sample with HRS after notching (visible NC), and (*c*) sample with LRS after notching (no NC).

The concept of an uphill quench is based on the rationale that, since residual stresses result from thermal gradients induced when the part is cooled, it is equally possible to develop thermal gradients and, consequently, residual stresses of an opposite nature by subjecting a cold sample to rapid heating. Residual stresses developed in this way counteract and tend to cancel the quenching stresses.

B. *Sample Preparation and Testing*

1. *Specimens*

The CT specimens were symmetrically machined after heat treatment to the dimensions of 95 × 91 × 10 mm (3.75 × 3.6 × 0.4 in.). One sample was machined to smaller dimensions, 40 × 38 × 10 mm (1.56 × 1.5 × 0.4 in.), from a large sample with HRS. Both sample configurations comply with ASTM E647. For material removal, an end mill was used for the edges, and a fly cutter was used for the reduction in thickness. A 0.15-mm (0.006-in.) diameter wire was used for the wire EDM notch. After the blanks were milled to the final size, they were scribed with reference marks at a spacing of 10 mm or 0.4 in. (5 mm or 0.2 in. on each side of the central line on the edge of the sample, as in Figure 1(a)). After the pin holes and the notch were machined, these reference lines were measured again to an accuracy of 2.5 μm (0.0001 in.), and the qualitative results are shown in Figures 1(b) and (c).

The notch length is 38 mm (1.5 in.), measured from the front face of the sample, and 19 mm (0.75 in.), measured from the pin holes.

2. *Residual-stress measurement through notch clamping*

Residual-stress levels were inferred from the displacement of the mating faces after the notch was cut into the CT specimens. These displacements were found to be compressive at the notch, in the range of 0.091 to 0.216 mm (0.0036 to 0.0085 in.) on different samples (different alloy compositions) after RT water quench, and in the range 0.000 to 0.041 mm (0.0000 to 0.0016 in.) after uphill quench. The sum of the scribe displacements for both halves of the CT specimens will be referred to as notch clamping (NC), which is used as a measure of the residual-stress level in the sample; the larger the NC, the higher the compressive residual stress.

During fatigue crack growth, the additional contribution of residual stress to the closure level is observed by examining the load-displacement records. The sample with LRS has less closure, which is due to other closure mechanisms (mainly roughness). These observations are presented in Figure 2. The crack closure measurements shown in Figure 2 cannot directly be used to partition the individual contributions to total closure, but they successfully capture the additional effects of residual stress.

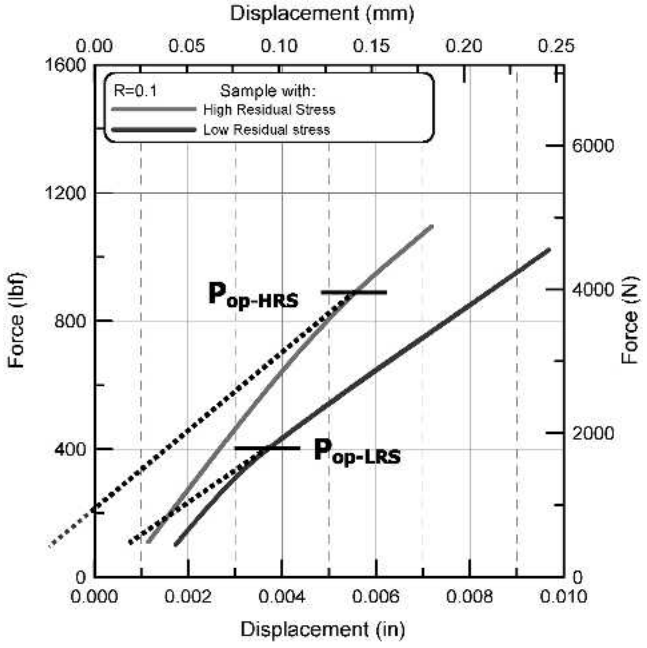

Fig. 2—Load-displacement records showing microstructure/roughness-induced closure (right curve) and the additional effect of residual stress on crack closure level (left curve). The P_{op} is the force required to fully open the crack under HRS and LRS conditions.

Low values of residual stress are not sufficient to overcome the effects of roughness-induced closure active in the vicinity of the crack tip. However, if residual stress is significant, then the crack tip can remain open while the surfaces near the notch are closed without an applied external force (bulge effect, as in Figure 3(a)). Therefore, the impact of roughness-induced closure is minimized, due to the fact that interference is no longer near the crack tip (specific to LRS samples, as in Figure 3(b)), and the height of the interfering features near the notch contributes less to the total crack closure level.

3. *The FCG testing*

The CT specimens were tested per ASTM E647 in RT 24 °C air with a relative humidity of 40 to 50 pct. The specimens

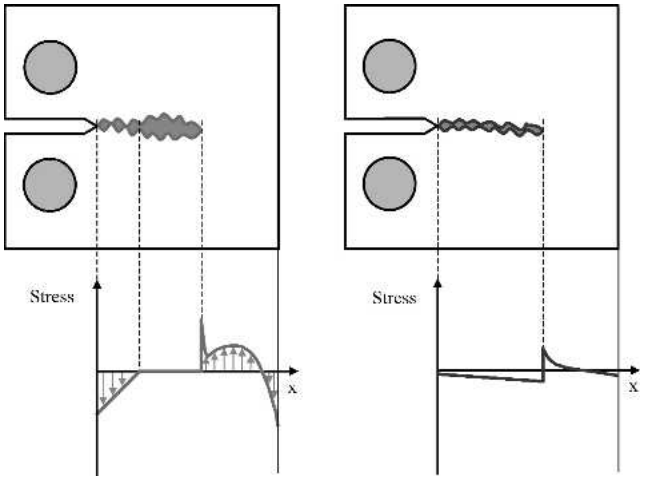

Fig. 3—Typical interference of the crack mating faces at minimum load. The schematic representation indicates: (*a*) HRS and (*b*) LRS conditions.

were tested under *K*-control, first under a decreasing crack-driving force range (Region I) to evaluate the thresholds, and then under an increasing crack-driving force range (Regions II and III). Above 10^{-3} mm/cycle, the test was continued using a shallower *K*-gradient to obtain the steeper region III data. The upper limit of the crack-driving force was assumed to be the "pseudo" (linear-elastic) fracture toughness of the materials (the CT samples in this study did not meet the plane-strain fracture-toughness requirements of ASTM E399; therefore, the measured fracture-toughness values are referred to as pseudo fracture-toughness values; plane-strain conditions were maintained until upper Region III, beyond which mixed-mode, plane-strain/plane-stress conditions occurred). The compliance technique was used to monitor the crack advance, and the frequency was set to 25 Hz (except in Region III, when the frequency was decreased to capture sufficient data points). All samples with both HRS and LRS were tested under both constant stress ratio, $R = 0.1$, and constant K_{max} (closure-free) conditions.

III. RESULTS AND DISCUSSION

A. *Determination of Residual-Stress-Free Thresholds from FCG Experiments on Specimens with HRS and LRS*

Paired samples from all alloys, one with HRS and the other with near-zero residual stress, were FCG tested ($R = 0.1$) under identical conditions. The results are presented in Figures 4(a) and (b). It is important to note that HRS curves have steeper slopes (higher *m* in Paris law: $da/dN = C(\Delta K)^m$), due to the proportionally higher residual-stress effects at lower-stress-intensity factor ranges, ΔK, a feature well captured by the log-log representation of the data.

Tests conducted on HRS samples were terminated prematurely, due to high closure levels, and the true thresholds were calculated by extrapolating the experimental data down to 10^{-7} mm/cycle. The other set of samples did not have residual-stress-induced closure; the only source of closure was the characteristic microstructural features of the alloys.

Thresholds of the HRS samples, 9 to 10 MPa$\sqrt{m}$ (8 to 9 ksi$\sqrt{in.}$) (Figure 4(a)), are unreasonably high for this type of cast aluminum alloys. Samples without residual stress (Figure 4(b)) show thresholds in the 3.5 to 5.5 MPa$\sqrt{m}$ (3 to 5 ksi$\sqrt{in.}$) range, a 100 pct difference, due to the presence of residual stresses (all the other parameters were kept constant). The increase in thresholds is explained by considering that the tip of the notch is subjected to compressive residual stresses (Figures 1(b) and 3(a)) that create a high degree of closure. Because of the high closure, less of the applied force physically acts on the crack tip (*i.e.*, sheltering of the crack tip occurs); therefore, a greater cyclic force is required to reach the threshold and to propagate the crack ($\Delta K_{th(compressive)}$), as in Figure 5(a). On the other hand, if the notch is found in a tensile-stress field (center crack-tension specimen, MT), the opposite effect is expected, as schematically presented in Figure 5(a). This behavior was observed by others,[7] for 7XXX-aluminum-alloy extruded rods. In this case, the thresholds ($\Delta K_{th(tension)}$) are lower than the residual-stress-free thresholds (ΔK_{th}), considering that the crack is open at all times, and the crack tip is exposed to the whole applied load range (Figure 5(b)).

By plotting threshold values *vs* NC for each tested sample and residual-stress level, a linear relationship was observed (Figure 6). This linearity holds true down to a critical value of the NC, below which the threshold remains constant and the sample can be considered residual-stress free; this is demonstrated by the plateau observed below a NC of 0.038 mm (0.0015 in.) for the 7 pct Si alloys. The critical NC is a function of the roughness level characteristic to the material: the lower the roughness, the lower the critical NC. Therefore, below a certain residual-stress level, the sample can be assumed residual stress free; the contact due to closure changes from "near the notch" to "near the crack tip," and closure mechanisms become mostly controlled by the intrinsic microstructural features of the alloy.

It is also observed in Figure 6 that closure-corrected, ΔK_{eff}, data (refer also to Section III.C.2) converge at low values of residual stress. This suggests that the variation in the residual-stress-free thresholds, ΔK_{th}, is mostly the result of microstructure effects causing differences in the roughness-induced closure.

Empirical relationships between threshold and NC (Figure 6) can be derived from FCG data. However, the development of such relationships requires for each material the knowledge of at least two residual-stress conditions necessary to obtain a linear fit. A better approach is to apply mathematical models to correct HRS data in a more general way. Thus, two mathematical models have been developed to account for the presence of residual stress directly from data with HRS. These two approaches are presented next and compared to the data from the residual-stress-free experiments.

B. *Mathematical Models to Account for Residual Stress*

1. *Restoring force model for clamping effect*

This model is designed to calculate the force required to restore the original notch spacing of the CT sample (Figure 7(b)), then use that force to compute the stress intensity due to the residual stress that caused that NC (Figure 7(a)). However, by restoring the original notch spacing, the surface of the sample

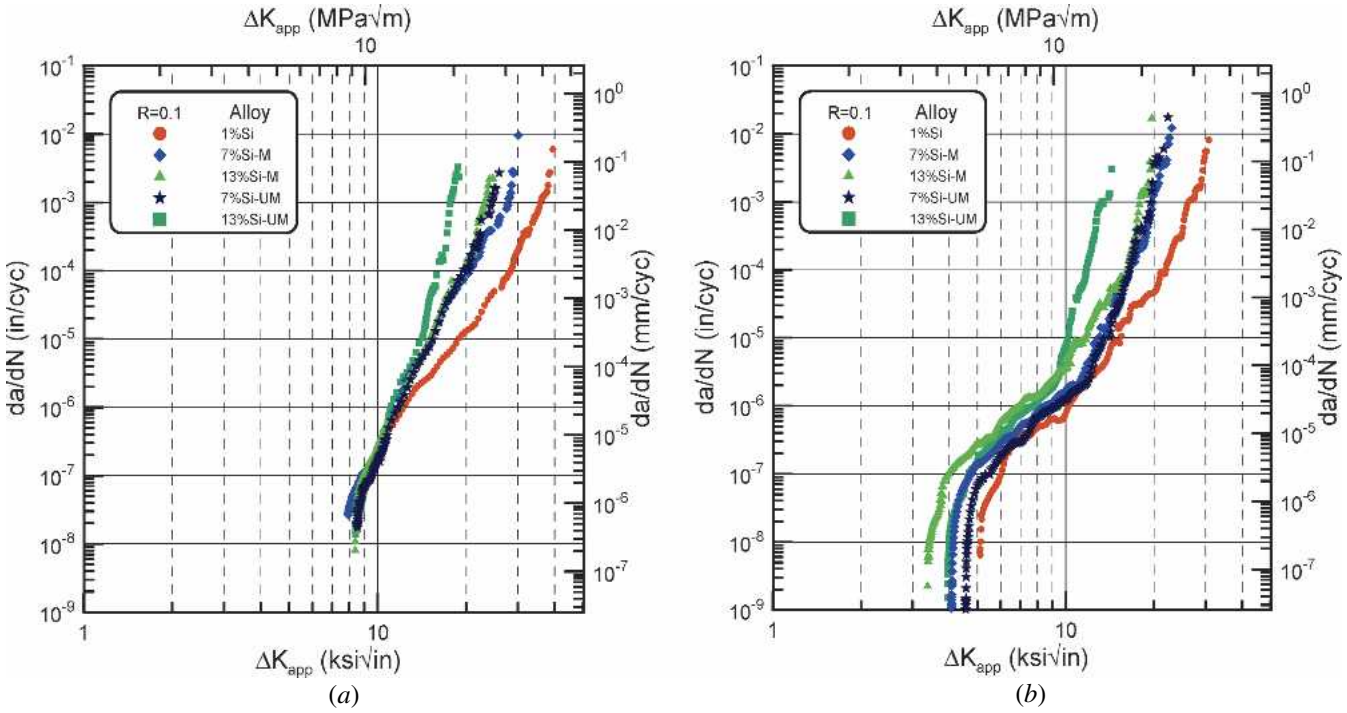

Fig. 4—The FCG curves for all alloys: (*a*) with residual stress and (*b*) without residual stress, under $R = 0.1$.

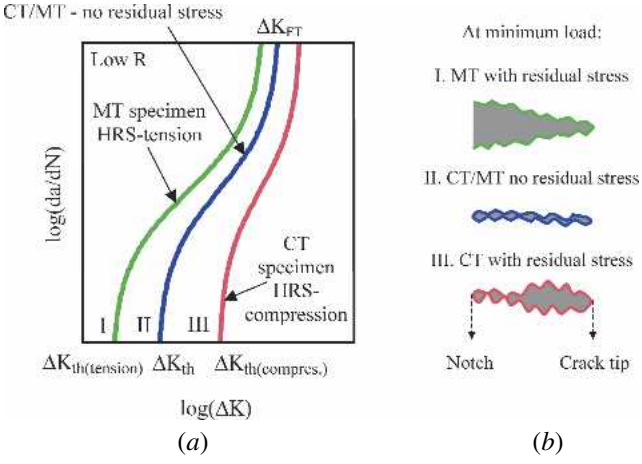

Fig. 5—The effects of compressive (CT specimen) and tensile (MT specimen) residual stresses on: (*a*) FCG behavior and (*b*) crack behavior at minimum load.

is physically forced from a compression state into a tension state, and the desired neutral state at the notch tip is not created. The equilibrium condition at the notch tip can be achieved by applying half of the force necessary to restore the original notch opening (Figure 7(c)).

The restoring force analysis used to calculate stress-intensity factors due to residual stress, K_{res}, is based on the two relationships shown in Eqs. [1] and [2], provided in Annex A1 of ASTM standard E647: (Note that a factor of 1/2 was included in Eq. [2].)

$$P = \frac{E \cdot \Delta\delta \cdot B}{m_1\left(\frac{a}{W}\right)} \qquad [1]$$

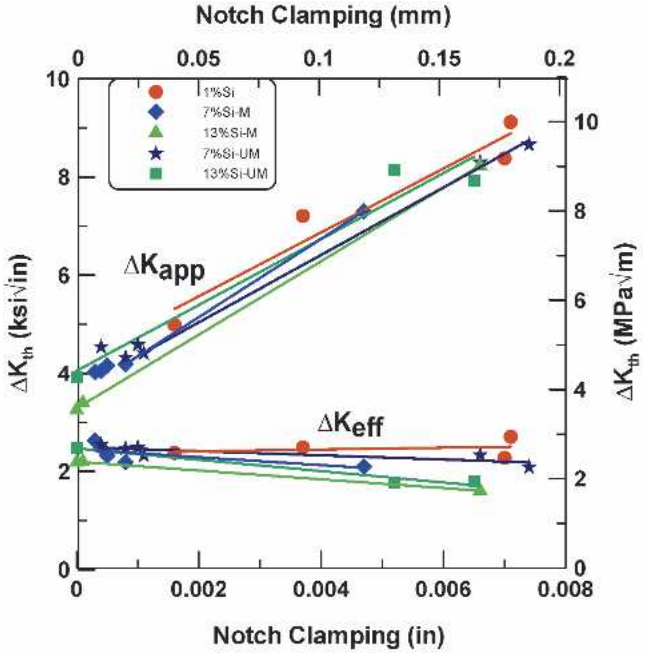

Fig. 6—The ΔK_{th} *vs* NC for applied-load conditions (ΔK_{app}) and closure-corrected conditions (ΔK_{eff}).

where

$$\frac{a}{W} = 1.00098 - 4.66951 \cdot u + 18.4601 \cdot u^2 - 236.825 \cdot u^3 + 1214.88 \cdot u^4 - 2143.58 \cdot u^5$$

$$u = \left\{\left[m_1\left(\frac{a}{W}\right)\right]^{\frac{1}{2}} + 1\right\}^{-1}$$

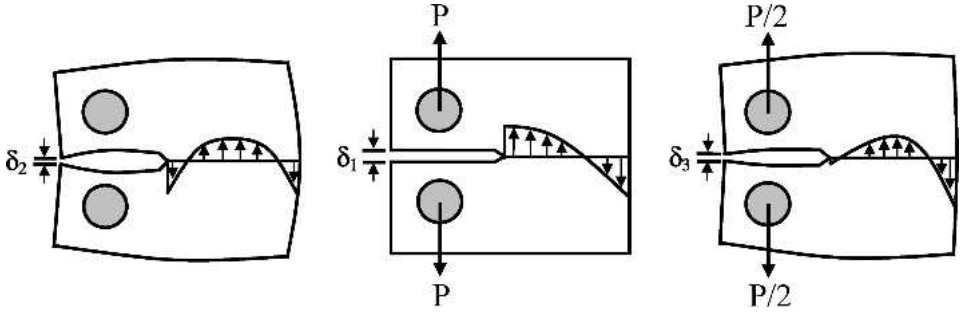

Fig. 7—The restoring force model: (*a*) the original residual-stress distribution, (*b*) the residual-stress distribution after restoring the original notch, and (*c*) the residual-stress-free notch tip.

The expression $m_1\left(\frac{a}{W}\right)$ is an iterative solution of the two equations above, which satisfies the value of $\frac{a}{W}$ specific to the given CT geometry, P = the load applied at the pin holes, E = Young's modulus, B = CT specimen thickness, W = CT specimen width (from pin holes), a = crack length (from pin holes), $\Delta\delta$ = change in notch (mouth) opening,

and
$$K_{\text{res}} = \frac{1}{2} \cdot \frac{P \cdot m_2\left(\frac{a}{W}\right)}{B \cdot \sqrt{W}} \qquad [2]$$

where K_{res} = the stress-intensity factor due to residual stress

$$m_2\left(\frac{a}{W}\right) = \frac{2 + \frac{a}{W}}{\left(1 - \frac{a}{W}\right)^{\frac{3}{2}}}\left[0.886 + 4.64 \cdot \frac{a}{W} - 13.32 \cdot \left(\frac{a}{W}\right)^2 + 14.72 \cdot \left(\frac{a}{W}\right)^3 - 5.6 \cdot \left(\frac{a}{W}\right)^4\right]$$

For the CT geometry used in this study, $a/W = 0.25$ at the beginning of the test, and the value of the stress-intensity factor due to residual stress, K_{res}, is calculated using Eqs. [1] and [2] as

$$K_{\text{res}} = \frac{1}{2} \cdot \frac{E \cdot \Delta\delta \cdot m_2\left(\frac{a}{W}\right)}{m_1\left(\frac{a}{W}\right) \cdot \sqrt{W}} \qquad [3]$$

It has to be noted that closure is the result of the combined effects of residual stress and microstructure/roughness. When residual stress is high, it dominates closure mechanisms; for LRS, the controlling closure mechanism is roughness. The lower the yield strength of the material, the higher the roughness of the fracture surface and the higher the residual-stress level below which closure becomes microstructure controlled. In other words, in low-yield/high-roughness materials, microstructure effects become active at higher residual-stress levels than in materials with high-yield strength. In the former category, corrections down to zero residual stress (or zero NC) are not needed and can lead to overcorrections beyond residual stress, eliminating microstructure effects. Similarly, high-yield/low-roughness materials can be undercorrected when residual-stress corrections down to zero are applied. In this study, for the high-roughness alloys (1 pct Si), a correction down to a NC of 0.038 to 0.064 mm (0.0015 to 0.0025 in.) is sufficient to consider the samples to be residual stress free. Alloys with 7 pct Si require a correction down to 0.025 to 0.038 mm (0.0010 to 0.0015 in.) NC, and the eutectic alloys (13 pct Si) down to 0.000 to 0.013 mm (0.0000 to 0.0005 in.). For simplicity, an average NC of 0.038 mm (0.0015 in.) was uniquely selected as a lower-bound value for all materials (using 7 pct Si as a baseline); below this value, residual stress-free conditions are assumed, and microstructure becomes the principal source of closure. For low-initial-residual-stress levels, no corrections are needed.

In general, however, when there is insufficient knowledge about the material, the microstructure/roughness-induced closure is not well characterized and the specimen-size/residual-stress relations are not known; in that case, a conservative correction down to zero residual stress is advisable.

The results of the restoring force correction are presented in Figures 8(a) and (b). Good agreement with the experimental data from residual-stress-free samples (Figure 4(b)) can be observed.

2. *Cut-compliance model for clamping effect*

This method targets the measurement of the residual stress and the residual-stress-intensity factor through the remaining ligament of a CT specimen. A slot or notch is successively extended through the part, and the resulting strain is measured at the appropriate location (displacements measured at the front face of the specimen are used in this study). This method is based on a fracture-mechanics approach that determines stress-intensity factors caused by the residual stresses with a very simple calculation.[24] The main benefit, similar to the previous model, is that it can evaluate the stress-intensity contribution from residual stress prior to a fatigue or fracture test, by measuring strains during the specimen preparation (during notch cutting, more precisely). This approach was successfully used and verified on CT specimens with residual stresses introduced by preloading the samples beyond yielding.[25] The method is based on small changes in notch displacement that are the result of small increments in crack length. In this study, the method was further simplified; specifically, residual-stress-intensity factors were correlated directly with the final notch length and the corresponding front-face-induced displacement (*i.e.*, the notch can be machined in one step instead of in successive steps).

The model treats the notch introduced to relieve residual stress as a mathematical crack. This approximation holds true for cracks with a depth-to-width ratio greater than five.[27] The

model, based on Castigliano's theorem, provides a very simple equation with which to calculate the stress-intensity factor, K_{res}, for a crack growing into a residual-stress field, as follows:

$$K_{res}(a) = \frac{E}{Z(a)} \cdot \frac{d\delta}{da} \quad [4]$$

where $Z(a)$ is an influence function that depends on both the geometry of the specimen (CT, in this work) and the location of the strain measurement (front face of the CT specimen, in this work). For a standard CT specimen with a crack depth of $a/W \geq 0.5$ and strain measurements taken at the back face, directly opposite to the cut, $Z(a)$ can be written as:[28]

$$Z(a) = -\frac{2.532}{(W-a)^{3/2}}$$

(CT specimen with back-face strain measurements) [5]

However, in this study, displacement measurements were taken at the front face where the cut was made (Figure 9), and thus a new expression for $Z(a)$ was developed.

The stress-intensity factor can be written in terms of the crack-driving force G and Young's modulus,[29] as

$$K^2 = EG = \frac{1}{2}\left(\frac{P_f}{BW}\right)^2 W \frac{d\left(\frac{E\delta B}{P_f}\right)}{d\left(\frac{a_f}{W}\right)} = \frac{1}{2}\frac{P_f}{B}E\frac{d\delta}{da_f} \quad [6]$$

where G = crack-extension force or elastic-energy-release rate; P_f = applied load at the front face; a_f, da_f = the crack length and the change in the crack length (from front face); and δ, $d\delta$ = the notch (mouth) opening and the change in the notch opening. Therefore,

$$E\frac{d\delta}{da_f} = \frac{2K^2B}{P_f} \quad [7]$$

From Eq. [4], the influence function can be written as

$$Z(a_f) = \frac{1}{K}E\frac{d\delta}{da_f} \quad [8]$$

Combining Eqs. [7] and [8], we get the expression of the influence function

$$Z(a_f) = \frac{2KB}{P_f} \quad [9]$$

Now, K can be written as[29]

$$K = \sigma_N\sqrt{b-a_f}\cdot F_2\left(\frac{a_f}{b},\frac{h}{b},\frac{d}{h}\right) = \left(\sigma_{N\text{-Tension}} + \sigma_{N\text{-Bending}}\right)\sqrt{b-a_f}\cdot F_2\left(\frac{a_f}{b},\frac{h}{b},\frac{d}{h}\right) \quad [10]$$

where F_2 = the parameter in Figure 10, b = the CT specimen width (from front face), h = the CT specimen half height, d = the distance notch-pin holes, σ_N, $\sigma_{N-\text{Tension}}$, and $\sigma_{N-\text{Bending}}$ = the applied stress, tension, and bending components

$$\sigma_{N-\text{Tension}} = \frac{P_f}{B(b-a_f)} \quad \text{and} \quad \sigma_{N-\text{Bending}}\frac{6P_f\left(a_f + \frac{b-a_f}{2}\right)}{B(b-a_f)^2} \quad [11]$$

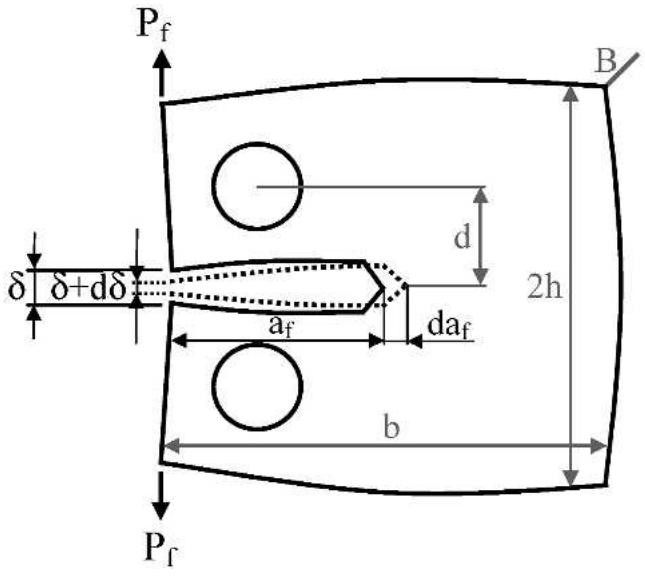

Fig. 9—The CT specimen (front-face-displacement measurements).

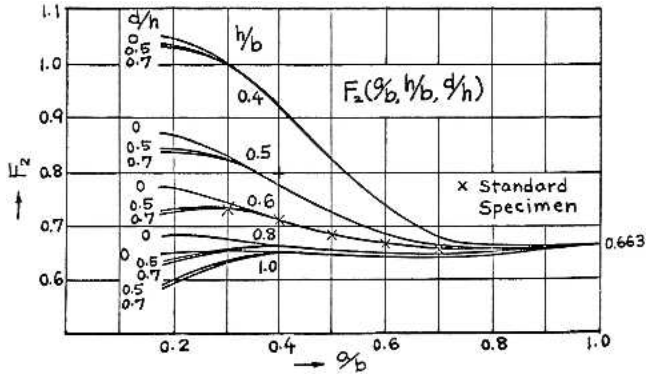

Fig. 10—Variation of F_2 parameter as a function of the specimen geometry.[29]

Using Eq. [11] in Eq. [10], K becomes

$$K = \left[\frac{2P_f(2b+a_f)}{B(b-a_f)^2}\right]\sqrt{b-a_f}\cdot F_2\left(\frac{a_f}{b},\frac{h}{b},\frac{d}{h}\right) \quad [12]$$

By introducing Eq. [12] in Eq. [9], $Z(a_f)$ can be determined as

$$Z(a_f) = \frac{4(2b+a_f)}{(b-a_f)^{3/2}}\cdot F_2\left(\frac{a_f}{b},\frac{h}{b},\frac{d}{h}\right) \quad [13]$$

Finally, the expression of the residual-stress-intensity factor for a CT specimen and strain/displacement measurements at the front face of the sample becomes

$$K_{res} = \frac{E}{Z(a_f)}\cdot\frac{d\delta}{da_f} = \frac{E}{\frac{4(2b+a_f)}{(b-a_f)^{3/2}}\cdot F_2\left(\frac{a_f}{b},\frac{h}{b},\frac{d}{h}\right)}\cdot\frac{d\delta}{da_f} \quad [14]$$

The F_2 can be determined using the chart presented in Figure 10.[29] For specimen geometries with $a/b > 0.4$, the d/h contribution is not significant, and Eq. [14] can be rewritten as

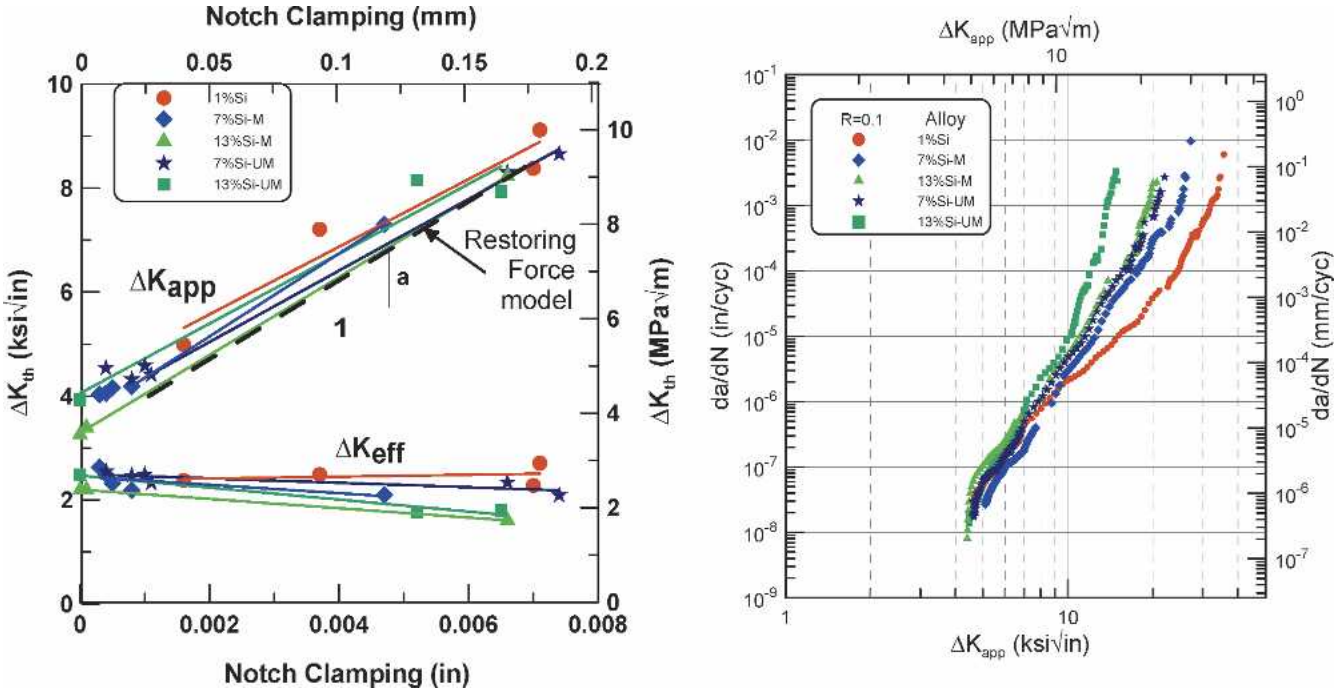

Fig. 8—(*a*) The ΔK_{th} *vs* NC and (*b*) the FCG curves of HRS samples after residual-stress correction using the restoring force model.

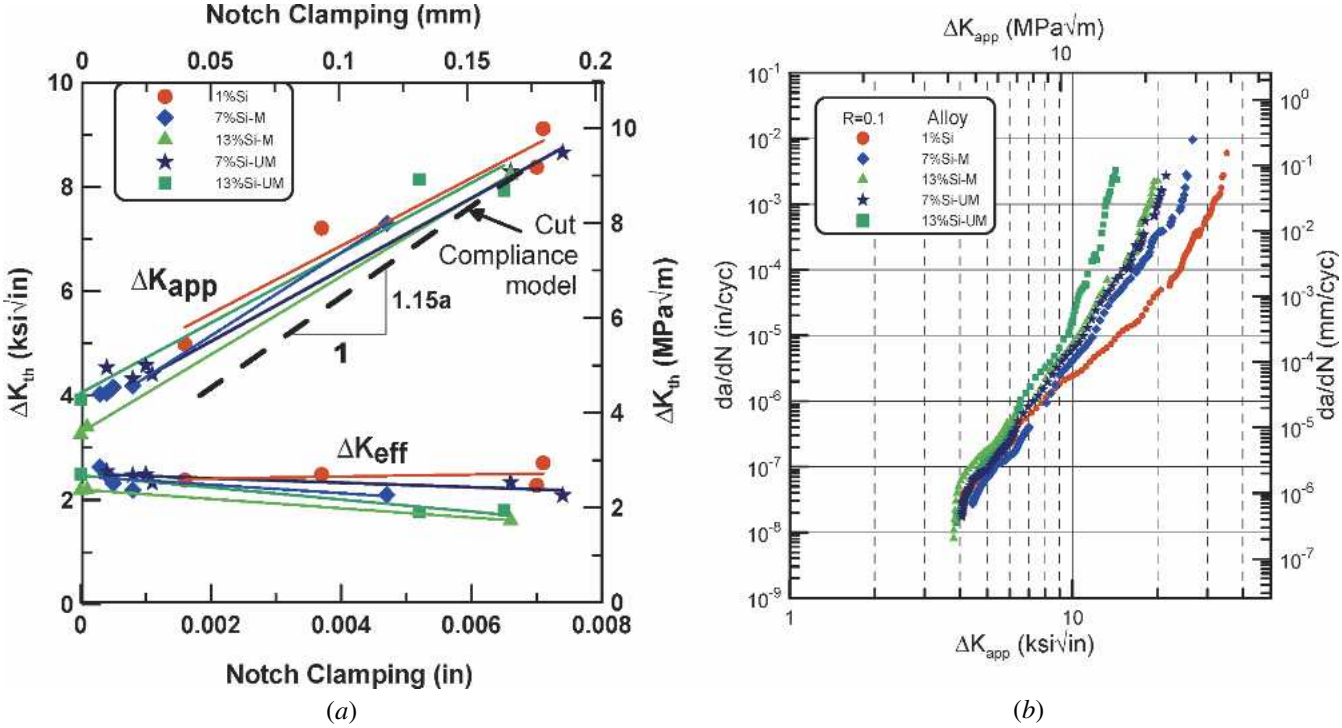

Fig. 11—(*a*) The ΔK_{th} *vs* NC and (*b*) the FCG curves of HRS samples after residual-stress correction using the cut-compliance method.

$$K_{res} = \frac{E}{\frac{4(2b + a_f)}{(b - a_f)^{3/2}} \cdot F_2\left(\frac{a_f}{b}, \frac{h}{b}\right)} \cdot \frac{d\delta}{da_f}$$

(CT specimen with front-face strain measurements) [15]

Thus, given the NC for a certain notch length, the stress-intensity factor due to the presence of residual stresses can be determined using Eq. [15].

The results of the corrections using the cut-compliance method are presented in Figures 11(a) and (b). A 15 pct difference was observed when comparing these results with the

restoring-force-model results; this means that stress-intensity factors are 15 pct lower. It must be noted that the cut-compliance method (Eq. [15]) requires the use of small-length increments and the resulting small-notch-displacements. In this study, however, the method used one large increment (the whole length of the notch), which introduces the observed differences. At the same time, the single increment makes the equation more user friendly, because cutting the notch in very small increments and calculating K_{res} for each successive step is laborious and impractical. On the other hand, the restoring-force model (Eq. [3]) can be applied in a single step; the results provided good estimates for stress-intensity factors due to residual stress and appropriate residual-stress corrections for various degrees of residual stress. Therefore, the restoring force method is recommended.

Both corrections for low-stress ratios, R (Figures 8(b) and 11(b)), were carried out using the following equation for the residual-stress-corrected stress-intensity factor range, ΔK_{corr}:

$$\Delta K_{corr} = K_{max} + K_{res} - K_{min} = \Delta K_{app} + K_{res} \quad [16]$$

The K_{res} correction was applied only to the maximum-stress-intensity factor, K_{max}, because when the crack is fully open, there is no contact, and the superposition principle is valid. However, applying the same correction to the minimum-stress-intensity factor, K_{min}, is not appropriate, since nonlinear contact in the crack wake has occurred due to other closure mechanisms, such as roughness. Consequently, the corrected stress-intensity-factor range, ΔK_{corr}, is reduced by the amount of K_{res}. It must be pointed out that Eq. [16] is valid when residual stresses are compressive and the stress ratio is low; these are conditions in which the minimum-stress-intensity factor, K_{min}, is below the stress-intensity factor that corresponds to the opening load, K_{op}, regardless of whether residual stress is present or not (in such cases, applying the correction to both K_{max} and K_{min} would result in no correction to ΔK, since residual stress is a mean stress effect). However, if the residual stresses were tensile or the stress ratios were sufficiently high, this assumption would not be valid.

In both correction models presented above, K_{res} was calculated based on the notch length alone, and the samples were tested after NC evaluations. Additional samples and castings were reserved for evaluating K_{res} through successive incremental saw cuts and NC measurements beyond the notch. The results for two machined samples (one with HRS and one with intermediate residual stress (IRS)) and one casting are shown in Figure 12.

The casting and the sample with HRS give nearly identical results, indicating that little residual-stress reduction occurred when the samples were machined from near-net-shape castings. The two corrective methods, the restoring-force model and the cut-compliance model, share similar behavior only at the initial notch length. The overall behavior of the two models is, however, different.

In this analysis, a constant K_{res} value was used for the full range of crack growth rates, a value calculated based on the initial notch length (Eqs. [3] and [15]). The assumption of a constant K_{res} is supported by three observations. First, it was observed that successive thresholds at different crack lengths have similar values, indicating that the effect of the residual stress was not diminished with the advance of the crack up to $a/W = 0.45$. Second, the restoring force model (Figure 12) shows a nearly constant value of K_{res} over the range of crack length used for crack growth testing. Third, although the cut-compliance method shows diminishing K_{res} with crack length, this approach is based on no contact of the mating faces. However, the additional clamping beyond the notch proves that contact (closure) will occur, raising the value of K_{res} above the cut-compliance-calculated value. In these conditions, it is evident that contact and closure compensate for the diminishing tendency of the residual stress with crack growth; therefore, it is appropriate to assume a constant K_{res} along the whole range of stress-intensity factors. The residual-stress-corrected data presented in Figures 8(b) and 11(b) are based on two constant K_{res} values calculated using the two mathematical models presented earlier.

C. *Testing Methods to Account for Residual Stress*

In addition to mathematical models, there are certain testing conditions (high-stress ratio or K_{max} = constant tests) or post-testing data processing techniques that can also provide closure-free data.

1. *The* K_{max} *= constant tests condition*

High-stress-ratio data were generated in an attempt to obtain a closure-free response. Tests under stress ratios up to 0.8 were terminated prematurely, due to high closure levels. In order to eliminate this problem, constant K_{max} tests (closure-free tests) were conducted. These test procedures resulted in stress ratios as high as $R \sim 0.9$ at threshold. Due to the fact that K_{max} remains constant, steep K-gradients can be used without the risk of crack growth retardation. Since K_{min} is increased as the crack advances, closure becomes less important, and it quickly disappears at lower values of ΔK.

The closure-free tests bring the thresholds down to 1 to 2 MPa$\sqrt{m}$ ($\sim$1 to 2 ksi$\sqrt{in}$.), since the faces of the crack are prohibited from interacting with each other and creating closure (Figure 13). As a result, both residual-stress-induced and roughness-induced closures become insignificant. However, this method has the disadvantage of being affected by second-order K_{max} effects.

2. *The* ΔK_{eff} *computation using closure-corrective methods*

In Figure 14, closure-corrected data are presented. The correction was done using the adjusted compliance ratio (ACR) method[30] for samples with HRS (Figure 4(a), before correction, and Figure 14(a), after correction) and LRS (Figure 4(b), before correction, and Figure 14(b), after correction).

The ACR method, like all the other closure-corrective methods, is a global (total)-closure-corrective technique, eliminating all types of closures (both residual-stress-induced and microstructure/roughness-induced closures). Comparing the FCG behavior (before closure correction) of samples with HRS (Figure 4(a)) and LRS (Figure 4(b)), a quantitative determination of residual-stress-induced closure effects on the FCG response can be performed. An additional comparison between the FCG behavior of samples without residual stress, before and after closure correction, leads to a quantitative evaluation of the effects of microstructure/roughness-induced closure (Figures 4(b) and 14(b)). Consequently, using successive comparisons of FCG data, quantitative determinations of both residual-stress and microstructure contributions to closure can be assessed, together with their effects on fatigue crack growth. To partition closure effects (residual stress and microstructure),

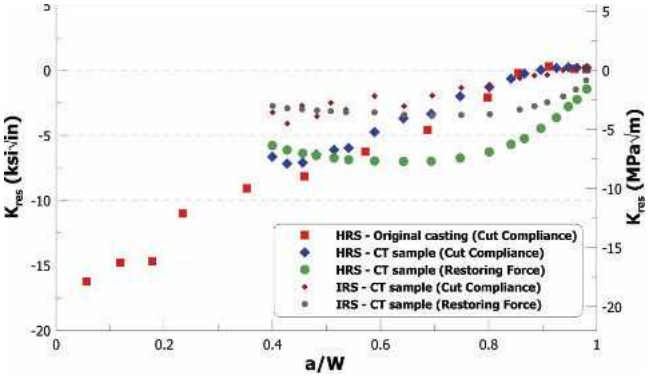

Fig. 12—Variation of K_{res} with crack length for HRS and IRS samples.

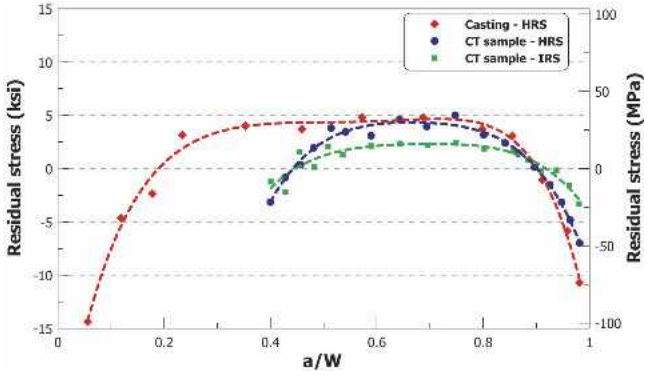

Fig. 16—Residual-stress profiles for a casting and two CT samples with HRS and IRS.

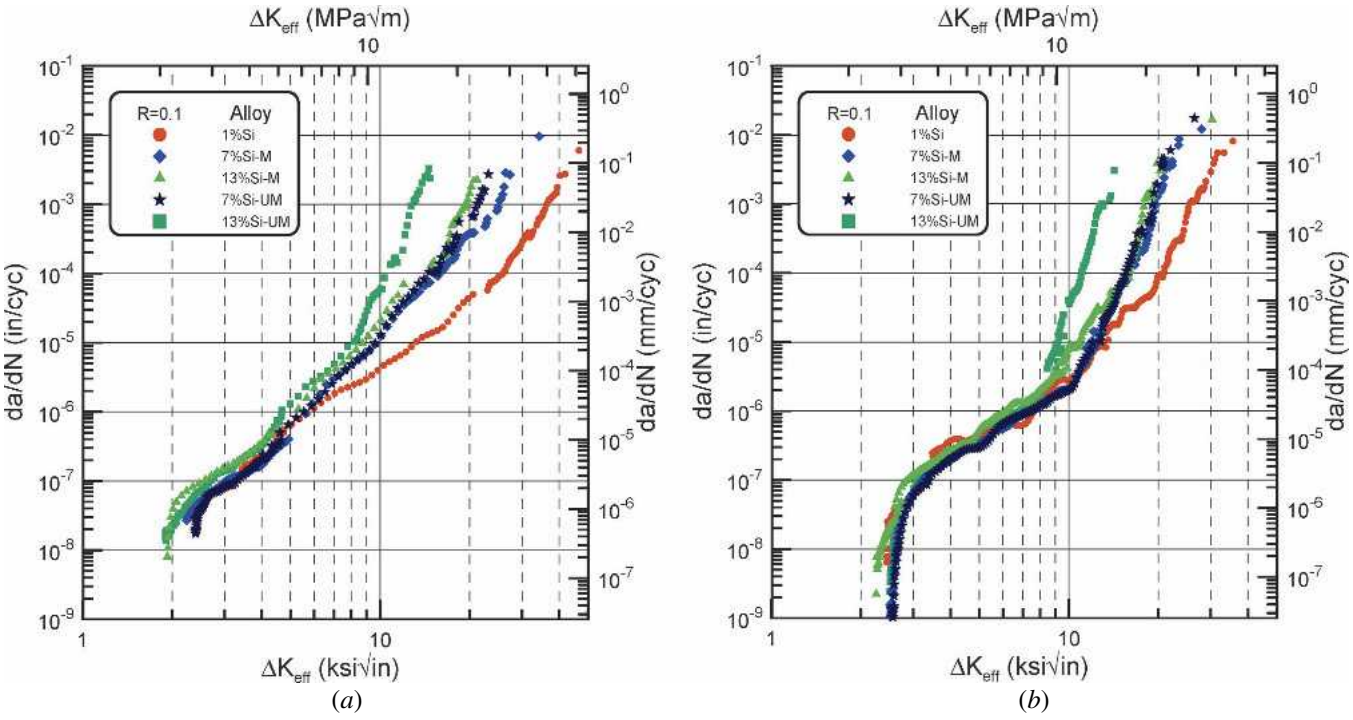

Fig. 14—The FCG data for all alloys after closure correction: (*a*) HRS and (*b*) LRS.

similar comparisons can be made between load-displacement records of samples with HRS and LRS.

D. *Procedures to Eliminate Residual Stress from CT Specimens*

To understand the real behavior of the material and to determine the effect of the residual stress, residual-stress-free samples of the same composition and mechanical properties need to be produced and compared with the samples with high residual stress. Several methods for producing residual-stress-free samples exist; two specific ones are introduced in the discussion that follows.

1. *Use of alternative quenching procedures (uphill quench)*

To significantly alleviate residual stress, the RT water quench, which is the main source of residual stress, needs to be replaced or adjusted. The usual quench (downhill) can either be done in a less severe medium, such as warm or boiling water, or be combined with a subsequent uphill quench.[26] The FCG data from uphill-quenched samples, shown in Figure 4(b), restored the thresholds (ΔK_{th}) to expected values for Al-Si-Mg alloys, 3.5 to 5.5 MPa$\sqrt{m}$ (3 to 5 ksi$\sqrt{in}$.). It should be noted that the difference in thresholds, and generally the difference in the whole FCG curve, between samples with residual stress (RT water quenched) and samples without residual stress (uphill quenched), is due entirely to the presence of residual stress (Figures 4(a) and (b)). By comparing the results of these two sets of experiments, the effect of compressive residual stresses can be quantitatively determined, and the corrective models introduced in Section III.B are validated. The accuracy of the mathematical models can be assessed by comparing Figure 4(b) with Figures 8(b) and 11(b).

2. *Use of smaller samples with LRS (cut from large samples with HRS)*

Another method for producing residual-stress-free samples is to machine specimens much smaller than the original size

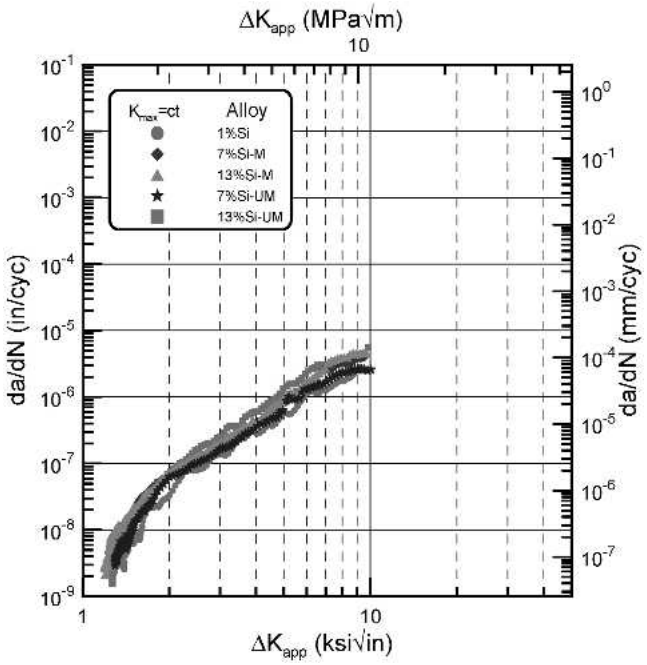

Fig. 13—The FCG results of K_{max} = constant (closure-free) tests.

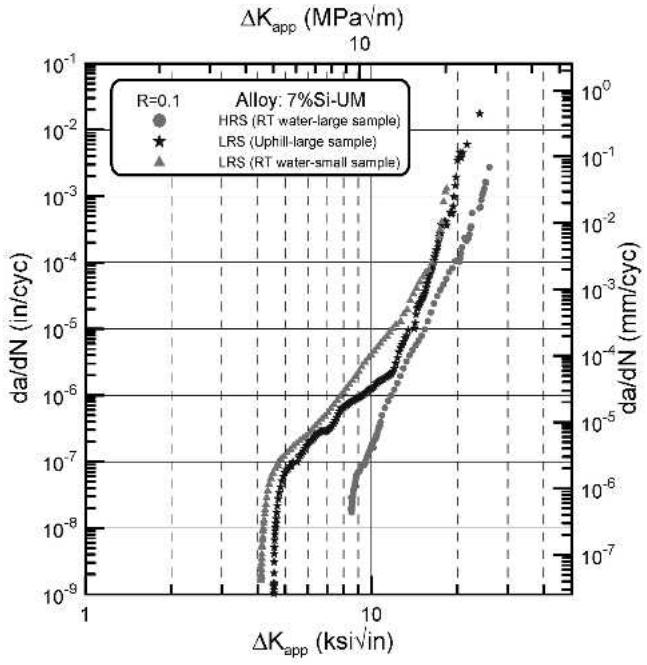

Fig. 15—Comparison between the FCG behavior of large samples with HRS and LRS and a small sample with LRS, after being cut from a large sample with HRS.

of the casting. It was found that by removing ~2/3 from the initial size casting, a residual-stress-free sample was obtained (Figure 15).

E. *Numerical Determination of Residual-Stress Profiles from* K_{res}

Using the cut-compliance method, by performing a series of successive cuts across the CT specimen ligament and recording the NC for every cut, a set of stress-intensity factors across the entire sample were calculated (Figure 12), using Eq. [15]. In this manner, a relationship between the stress-intensity factors due to residual stresses (K_{res}) and the actual values of the residual stresses present in the CT sample (σ_{res}) can be determined. The relationship $K_{res} - \sigma_{res}$ is based on weight function solutions, as shown in Eq. [17]:

$$K_{res}(a) = \int_{a_0}^{a} h(x,a)\sigma_y(x)dx \qquad [17]$$

Equation [17] can be solved for the residual stress (when K_{res} is known) by assuming that the stress, σ_j, is constant in each of the n intervals, between each a_{n-1} and a_n. Therefore, Eq. [17] can be rewritten in discrete form as

$$K_{res}(a_i) = \sum_{j=1}^{i} \sigma_j \int_{a_{j-1}}^{a_j} h(x,a_i)dx \qquad [18]$$

Slightly different formulations of the weight functions, $h(x,a)$, have been used by several researchers.[6,9,10,14,15,17] In this work, the weight function formulation for a CT specimen[31] was followed:

$$h(x,a_i) = \sqrt{\frac{2}{\pi a_i}} \frac{1}{\sqrt{1-\frac{x}{a_i}}} \left[1 + \frac{1}{\left(1-\frac{a_i}{W}\right)^{\frac{3}{2}}} \sum_{v,\mu} A_{v\mu} \left(\frac{a_i}{W}\right)^{\mu} \left(1-\frac{x}{a_i}\right)^{v+1} \right] \qquad [19]$$

where coefficients $A_{v\mu}$ are listed in the Table I, and a_i are cuts measured from the load line (pin holes).

Table I. The $A_{v\mu}$ Coefficients in Equation [19][31]

v/μ	0	1	2	3	4
0	2.673	−8.604	20.621	−14.635	0.477
1	−3.557	24.9726	−53.398	50.707	−11.837
2	1.230	−8.411	16.957	−12.157	−0.940
3	−0.157	0.954	−1.284	−0.393	1.655

The mathematical approach is complex and it requires numerical integration, but once solved, the residual-stress distribution can be quantified and a relationship NC-residual-stress level can be established. This equation was used by others to determine the residual-stress distribution in a CT sample overloaded prior to the cuts.[25] In the present study, residual stress was a pre-existing condition (introduced during quenching) before the notch was cut, but the stress distribution was determined in the remaining ligament after the notch was machined.

This approach allows each σ_j to be uniquely determined, and the numerical results are given in Figure 16.

Residual-stress profiles are consistent with the expectation that the surface has compressive stresses, while the interior is in tension. For both the casting and the CT samples, the residual stress in the interior is fairly uniform and is lower in absolute value than the surface compression. This is expected, because the thermal gradients due to quenching are

greater at the surface than in the interior. The stress distribution in the CT specimens represents, in fact, the residual-stress profile after the notch has been cut, just before testing.

It is important to emphasize that a tensile residual-stress value of 5 ksi in the interior of a sample would not commonly be considered very high (although it is much higher on the edge of the sample). However, there are two reasons why such a level of residual stress is critical for long-crack threshold data. First, in the presence of residual stress, the larger the sample size relative to the original size of the part, the greater the degree of remnant residual stress in the machined sample (see the differences between the large and the small samples in Figure 15). Second, the larger the sample and crack size, the smaller the applied stress for a given stress intensity. These two points combine to amplify the effect of residual stress on long-crack growth data. If data were being generated on samples with real flaw sizes and at real stress levels, the impact of residual stress on the crack growth rate behavior would be greatly reduced, possibly to the point of insignificance. Thus, a good understanding of these phenomena and their implications on both small and long cracks are critical for design.

There is a direct correlation between NC and residual-stress amplitude that can be observed by analyzing the residual-stress profiles of CT samples with different degrees (high and intermediate) of residual stress in Figure 16. A two-times-larger NC (0.193 mm/0.0076 in. for HRS *vs* 0.091 mm/0.0036 in. for IRS) leads to approximately double maximum tensile and also maximum compressive residual-stress amplitudes.

It has to be noted that the methodology presented in this article is two-dimensional (2-D). For the CT specimens evaluated in this study, sufficient material was removed from the thickness during the sample preparation (5 mm/0.2 in. on each side) so that the through-the-thickness variation in residual stress was negligible. This assumption was further confirmed by the experimental observation that the crack fronts did not indicate any evidence of crack tunneling (bowing), a common indicator of through-the-thickness residual stress. Moreover, the compliance and K solutions are 2-D solutions, and there are no mathematical tools to account for the third dimension.

In addition, it needs to be pointed out that residual-stress corrections to ΔK are valid when residual stresses are compressive and the stress ratio is low (*i.e.*, the minimum stress-intensity factor, K_{min}, is below the stress-intensity factor corresponding to the opening load, K_{op}, whether or not residual stress is present). If the stress ratio is high, residual-stress corrections to ΔK will not be appropriate, because applied and effective stress-intensity factor ranges will be similar. However, instead of closure, second-order K_{max} effects can still shift the data to a lesser extent. Also, when the initial residual stresses are tensile instead of compressive, such residual-stress corrections are not appropriate.

IV. CONCLUSIONS

1. When present, residual stress can bias the true response of the base material and mask the influence of the characteristic microstructural features of the material.
2. The effect of residual stress on crack growth rates is most pronounced at low ΔK levels (near-threshold regime), at which the applied stresses are low and, therefore, the ratios of residual stresses to applied stresses are high. Fracture toughness is also affected by similar residual stresses, but due to high applied stresses, the effect is considerably diminished relative to the impact on threshold.
3. Clamping measurements before and after notch cutting are good indicators of the residual-stress severity. There are also other good testing indicators, such as closure measurements through load-displacement records. However, these records cannot directly separate the effect of residual-stress-induced closure from microstructure-induced closure.
4. Through the evaluation of experimental results with both HRS and LRS, two mathematical models were validated to adequately quantify the effect of residual stress on FCG data. The corrective methods apply to specimen geometries for which NC can be measured (*i.e.*, edge-crack-type specimens, such as CT) as well as to cases in which residual-stress distribution is symmetrical (compression on the surface and tension in the interior).
5. Quantifying residual-stress effects on FCG data is insufficient for accurately characterizing the intrinsic microstructural characteristics of the material. For that purpose, residual-stress-free samples are needed. Methods for reducing residual stress include thermal stress-relieving techniques and the proper selection of specimen geometry, size, and location (from the original casting), to preserve the symmetry of the residual-stress profile.
6. When residual stress is under certain critical values, NC is small, and it can be ignored; the bulge effect is not operative and intrinsic microstructural closure effects are dominant. At high levels, residual stresses mask microstructure effects, and mathematical corrections need to be applied.
7. Because of the significant impact of residual stress on fatigue crack propagation data, consideration should be given to reviewing and revising ASTM E647 specifications to include the reporting of NC measurements on the testing specimens and to provide appropriate methods for residual-stress compensation. For correct interpretation of FCG response, NC measurements as well as crack growth data before and after residual-stress correction ought to be reported.
8. The new restoring-force technique introduced in this article can be utilized to address and quantify the effects of residual stress on the FCG behavior of any material and specimen size, and for any magnitude of residual stress, assuming symmetrical residual-stress distributions. Additional investigations need to be conducted to assess the validity of the model in asymmetric cases.

ACKNOWLEDGMENTS

Special thanks go to Mr. Keith Donald for his important contribution to this work, on critical issues related to the impact of residual stress on fatigue crack growth. The authors express their thanks to General Motors Corporation (GM) for partly supporting the FCG testing, to the Alcan Corporation for providing high-purity aluminum, and to the Palmer Foundry for preparing the sand molds needed in this work. The authors are indebted and thank Dr. Peggy Jones of GM and Dr. Fred Major of Alcan for their sustained support and valuable technical assistance.

REFERENCES

1. T. Hanabusa and H. Fujiwara: *Proc. 32nd Jpn. Congr. Res*., 1989, pp. 27-36.
2. G.E. Dieter: *Engineering Design*, 3rd ed., McGraw-Hill Book Co., New York, NY, 2000.
3. C.O. Ruud: in *Residual Stress Effects in Fatigue*, ASTM STP 776, ASTM, Philadelphia, PA, 1982, pp. 3-5.
4. D. Walker: *Adv. Mater. Processes*, 2001, Aug., pp. 30-33.
5. L. Mordfin: in *Residual Stress Effects in Fatigue*, ASTM STP 776, ASTM, Philadelphia, PA, 1982, pp. 6-12.
6. G. Glinka: in *Fracture Mechanics*, ASTM STP 677, ASTM, Philadelphia, PA, 1979, pp. 198-214.
7. R.J. Bucci: in *Fracture Mechanics-13th Conf*., ASTM STP 743, ASTM, Philadelphia, PA, 1981, pp. 28-47.
8. G.E. Nordmark, L.N. Mueller, and R.A. Kelsey: in *Residual Stress Effects in Fatigue*, ASTM STP 776, ASTM, Philadelphia, PA, 1982, pp. 44-62.
9. A.P. Parker: in *Residual Stress Effects in Fatigue*, ASTM STP 776, ASTM, Philadelphia, PA, 1982, pp. 13-31.
10. D.V. Nelson: in *Residual Stress Effects in Fatigue*, ASTM STP 776, ASTM, Philadelphia, PA, 1982, pp. 172-94.
11. W. Geary and J.E. King: *Int. J. Fatigue*, 1987, vol. 9, pp. 11-16.
12. G.A. Webster and A.N. Ezeilo: *Int. J. Fatigue*, 2001, vol. 23, pp. S375-S383.
13. S. Sirtori and L. Vergani: *Met. Sci. Technol*., 1988, vol. 6, pp. 40-46.
14. Y.C Lam and K.S. Lian: *Theor. Appl. Fract. Mech*., 1989, vol. 12, pp. 59-66.
15. M. Beghini and L. Bertini: *Eng. Fract. Mech*., 1990, vol. 36, pp. 379-87.
16. R.W. Bush, R.J. Bucci, P.E. Magnusen, and G.W. Kuhlman: in *Fracture Mechanics-23rd Symp*., ASTM STP 1189, ASTM, Philadelphia, PA, 1993, pp. 568-89.
17. S.R. Daniewicz, J.A. Collins, and D.R. Houser: *Int. J. Fatigue*, 1994, vol. 16, pp. 123-33.
18. S.J. Maddox: *Int. J. Fract*., 1975, vol. 11, pp. 389-408.
19. R.D. Brown and J. Weertman: *Eng. Fract. Mech*., 1978, vol. 10, pp. 757-71.
20. W.O. Soboyejo and J.F. Knott: *Int. J. Fatigue*, 1990, vol. 12, pp. 403-07.
21. K. Tokaji and T. Ogawa: *Fatigue Fract. Eng. Mater. Struct*., 1990, vol. 13, pp. 411-21.
22. A.M. Korsunsky and P.J. Withers: *Key Eng. Mater*., 1997, vol. 127, pp. 1183-90.
23. C.N. Reid: *Scripta Metall*., 1988, vol. 22, pp. 451-56.
24. H.-J. Schindler: *Int. J. Fracture*, 1995, vol. 74, pp. R23-R30.
25. M.B. Prime: Fatigue *Fract. Eng. Mater. Struct*., 1999, vol. 22, pp. 195-204.
26. H.N. Hill, R.S. Barker, and L.A. Willey: *Trans. ASM*, 1960, vol. 52, pp. 657-74.
27. W. Cheng and I. Finnie: *J. Eng. Mater. Technol*., 1993, vol. 115, pp. 220-26.
28. H.-J. Schindler: in *Advances in Fatigue Crack Closure Measurement and Analysis-Second Volume*, ASTM STP 1343, ASTM, Philadelphia, PA, 1999, pp. 175-87.
29. H. Tada, P.C. Paris, and G.R. Irwin: *The Stress Analysis of Cracks Handbook*, 3rd ed., ASME, New York, NY, 2000.
30. G.H. Bray and J.K. Donald: in *Advances in Fatigue Crack Closure Measurement and Analysis*, vol. 2, ASTM STP 1343, ASTM, Philadelphia, PA, 1999, pp. 57-78.
31. T. Fett and D. Munz: *Computational Mechanics Publications*, Southampton, United Kingdom, 1997.